International Journal of Heat and Fluid Flow 29 (2008) 665–674

Contents lists available at ScienceDirect

International Journal of Heat and Fluid Flow

journal homepage: www.elsevier.com/locate/ijhff

Study of scalar macro- and microstructures in a confined jet

Nikolai Kornev *, Valery Zhdanov, Egon Hassel

Lehrstuhl für Technische Thermodynamik, Universität Rostock, A. Einstein Strasse 2, 18059 Rostock, Germany

ARTICLE INFO

Article history:
Received 2 November 2007
Received in revised form 5 March 2008
Accepted 8 March 2008

Keywords:
Mixing
Passive scalar
Dissipation rate
Intermittency
Anisotropy
Multifractals

ABSTRACT

The scalar structures in a confined jet are studied at high Reynolds and Schmidt numbers. Both flow modes without the recirculation zone (jet mode) and with the massive separation and creation of the recirculation zone (r-mode) are considered. Despite of the big difference in the flow modes, the fine scale scalar structures gained from highly resolved PLIF measurements possess similar statistical properties such as the normalized cumulative distributions and probability densities of the dissipation rate. The fine scalar structures are distributed nearly uniformly in space with the scalar gradient vector having a slight preference to align with the most compressive mean strain axis. The scalar field exhibits small-scale intermittency which is strongly dependent on the flow mode. The intermittency is most pronounced in the front of the recirculation zone and becomes weaker on the centerline and downstream. The most contribution to the scalar variance is made by large scale motions whereas the contribution of fine scales smaller than typical inertial range scales is negligible. Examination of the multiplier distributions has not supported the concept of the multifractal nature of the scalar dissipation field.

1. Introduction

Mixing in coaxial confined jets has been investigated for a long time because of many practical engineering applications in, e.g. combustion chambers, injection systems, chemical mixing devices and many others. In this paper the coaxial axisymmetric jet mixer consisting of a nozzle of diameter d positioned along the center line of a pipe of diameter D has been considered (see Fig. 1). The fast inner jet (water) with the bulk velocity U_d is confined by a slower outer coflow (water) with velocity $U_D \ll U_d$. The most important parameters determining the mixing process are the flow rate ratio $\dot{V}_D/\dot{V}_d$, the diameter ratio D/d and the Reynolds number $Re_d = dU_d/\nu$.

Most publications on confined jets are devoted to the study of large scale effects in configurations in which the inner jet is much slower than the coflow $U_d/U_D \ll 1$ (see, for instance, Rehab et al., 1997; Mortensen et al., 2003; Lima and Palma, 2002). These investigations are motivated by two important applications: stabilization of flame fronts by swirl burners and the saturation of air coflow with molecules of substances transferred by the internal jet. Rehab et al. (1997) revealed and investigated sustaining low-frequency pulsations caused by the recirculating flow cavity arising on the axis in the inner jet region. The structure of this reverse flow zone is similar to the well known wake-type structure behind bluff bodies. Similar phenomena are discussed in this paper for the case of confined coaxial jets with $U_d/U_D \gg 1$ in which the reverse flow region is not on-axis but near the wall. Surprisingly, the case $U_d/U_D \gg 1$ has attracted less attention although this flow mode is very important for homogenization devices and free jet reactors. Two different flow modes can be observed in jet mixers, depending on the flow rate ratio $\dot{V}_D/\dot{V}_d$ (see Barchilon and Curtet, 1964). If $D/d < \beta(1 + \dot{V}_D/\dot{V}_d)$, where $\beta \approx 1$ is an empirical constant found from a simple entrainment model, the flow is similar to a free jet (henceforth referred to as jet-mode or j-mode for short). If $D/d > \beta(1 + \dot{V}_D/\dot{V}_d)$ a strong flow separation at the pipe walls results in a recirculation zone (see Fig.7 in Zhdanov et al., 2006) behind the nozzle (henceforth referred to as recirculation-mode or r-mode for short). A qualitative description of the r-mode is given by Barchilon and Curtet (1964). The large scale flow phenomena in a jet mixer has been the subject of our previous experimental and numerical works (see Kornev et al., 2005; Zhdanov et al., 2006; Hassel et al., 2006; Tkatchenko et al., 2007). Our study showed that the flow in the r-mode is highly unsteady and time averaged results do not describe properly the true nature of flow phenomena typical for this mode. The presence of long period temporal oscillations with a sort of opposition-of-phase of the flow is revealed and quantified. In the Section 3.1 we explain the physical mechanism causing such oscillations. The LES (large eddy simulation) model used in the present study is described in details in Tkatchenko et al. (2007).

Formation and dynamics of fine scalar structures in liquids at high Schmidt $Sc \sim 10^3$ and Reynolds numbers belongs to the most complicated fields of fluid mechanics. The resolution required for such a study is of the order of the Batchelor scale, defined as $\eta_B = \eta/\sqrt{Sc}$, where η is the Kolmogorov scale. For the full developed turbulent liquid flows, the Batchelor scale becomes so tiny that it is

* Corresponding author. Tel.: +49 381 498 9407; fax: +49 381 498 9402.
E-mail address: nikolai.kornev@uni-rostock.de (N. Kornev).

0142-727X/$ - see front matter © 2008 Elsevier Inc. All rights reserved.
doi:10.1016/j.ijheatfluidflow.2008.03.011

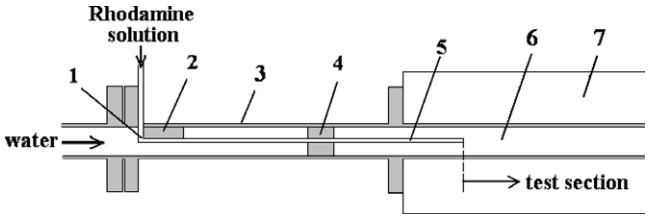

Fig. 1. Sketch of the flow: 1, knee bend of nozzle; 2, plate for damping of vortices shed from knee bend 1; 3, outer tube; 4, support plates; 5, nozzle; 6, test section; 7, water box.

hard to perform the DNS (direct numerical simulation) at reasonable computer costs. Some success has been achieved by DNS only for moderate *Re* and *Sc* numbers (see, for example, Schumacher and Sreenivasan, 2005; Kushnir et al., 2006). Experimentally, using modern PIV (particle image velocimetry) and PLIF methods researchers are capable of penetrating into the range of fine scales comparable with Batchelor ones. Most of the experimental progress in the field of scalar turbulence at high Schmidt numbers has been achieved by the group of Dahm (see, for example, Buch and Dahm, 1996). The three-dimensional measurement technique for scalar fields has been developed by Su and Clemens (2003) and Southerland and Dahm (1994). The state of the art in this field can be found in Su and Clemens (2003). The scalar dissipation rate determination is one of the most important aims of measurements. This procedure is complicated since it requires calculation of gradients. In this case the effects of the data processing, such as the smoothing filter and numerical stencil, are significant and must be considered. A detailed consideration of the accuracy assessment of scalar dissipation measurements is given by Wang et al. (2007).

The main focus of the present paper is the study of fine structures of passive scalars in the liquid phase using highly resolved PLIF (planar laser-induced fluorescence) measurements. The following questions are considered in the paper:

- What kind of flow structures are responsible for the appearance of sustaining low-frequency oscillations in the r-mode? Why are the oscillations nearly antisymmetric?
- What kind of scalar microstructures are created in a confined jet?
- What are the statistical properties of the microstructures in different flow modes?
- How does the intermittency of the scalar field behave along the jet for different flow modes?
- What is the preferential orientation of the scalar microstructures?
- Which scales do make the main contribution to the scalar variance?
- Does the scalar dissipation field exhibit the multifractal properties ?

The paper is organized as follows. Section 2 briefly describes the experimental facility. Section 3.1 reports the peculiarities of the macroflow and explains the physical mechanisms behind the longitudinal oscillations in the jet mixer under consideration. The rest of the paper (Sections 3.2–3.8) focuses on the study of the fine scalar structures. A special attention is paid to the problems which solution can be useful for further development of theoretical models capable of mixing modelling at high *Sc* numbers (Sections 3.6–3.8). Conclusions are presented in the final section.

2. Experimental facility

The flow field investigated here is the turbulent axisymmetric jet developing in a coflow confined by a pipe of diameter $D = 50$ mm and length 5000 mm. A schematic of this flow system is given in Fig. 1. Medium in both flows was water ($Sc \sim 10^3$). The inner tube 5 had diameter $d = 10$ mm and the length 600 mm chosen from the condition that perturbations caused by the knee bend are suppressed near the nozzle exit. The test section of the mixer was installed in a Perspex rectangular box filled with water to reduce refraction effects. More detailed information about the hydrodynamic channel can be found in Zhdanov et al. (2006). Since the Reynolds number based on the jet exit velocity U_d is $Re_d = dU_d/\nu = 10^4$ the jet can be considered as a fully- developed turbulent jet. Two sets of measurements with the recirculation zone and without it have been performed. Table 1 lists the experimental conditions for each set. A scalar field was measured by the planar LIF method. The turbulent jet contains a fluorescing substance (Rhodamine 6G) with a concentration of 0.5 mg/l. In experimental measurements, to prevent changes in the flow background intensity due to contamination of water by the Rhodamine solution, the charged coflow vessels and the vessels collected mixture behind the test section were separated. The *x*-axis of the coordinate system is aligned along the pipe centerline downstream. The coordinates *y* or *r* are measured from the *x*-axis. The point $r/D = 0$ or $y/D = 0$ means that the centre of the measurement window is on the mixer axis. Measurements were performed at positions ranging from $x/D = 0.1$ to $x/D = 9$ downstream of the nozzle exit. A measuring system comprised a Nd:YAG laser operating at a wavelength of 532 nm and with a pulse duration of 7 ns, a sensicam qe camera (1376 × 1040 pixel, 19.8 fps, exposure times 500 ns) with a K2 long-distance microscope system, and an optical unit to make a laser sheet. The binning 4 × 4 was applied to improve the quality of measurements. The use of the K2 system equipped with the objective CF-2 enables to record the scalar field in the window of 2.74 × 2.075 mm with a spatial resolution up to ~31 μm. The resolution has been fixed using USAF target at the measurement conditions. The laser sheet was formed vertically along the mixer axis by two convex lenses of 200 mm and 100 mm focus lengths, a concave lens of (−50) mm focus length and a cylindrical lens of (−250) mm focus length. The laser sheet thickness has been estimated using the beam generated by the diode continuum laser DD532-25-3 (Picotronic GmbH) at the same length 532 nm as the Nd:YAG laser. The thickness measurements performed with the Beam Scan (model 11801, Photon Inc.) indicate that the laser thickness doesn't exceed 40 + 8 μm within the measurement window. Since the laser beam quality of the diode laser is worse than that of the impulse laser Nd:YAG (Continuum, PREC II 8000) it is assumed that the laser thickness used in further experiments with Nd:YAG lies within the same range.

Time resolution was limited by the 10 Hz frequency of laser used as an external trigger of the camera. Mixture fraction distributions *f* were calculated from the emitted Rhodamine intensity distributions *I* referred to the maximum intensity I_0 determined on the centerline in the first cross-section at $x/D = 0.1$. The measurements at each cross-section x/D produced a data volume composed of 3000 successive highly resolved two-dimensional spatial data planes arranged sequentially in time. Each data plane is, in turn, composed of an array of 344 × 260 individual point measurements of the local conserved scalar field value *f*.

Following the suggestion from Buch and Dahm (1996), the derivatives of the function *f* were calculated using the Sobel

Table 1
Parameters of experiments

Flow mode	$U_d(ms^{-1})$	$U_D(ms^{-1})$	$\dot{V}_D/\dot{V}_d$
r-mode	1.0	0.06	1.3
j-mode	1.0	0.1	5.0

operator with two 3×3 kernels which are convolved with the original image to calculate approximations of the derivatives:

$$\left(\frac{\partial f}{\partial x}\right)_{i,j} = \frac{1}{8\Delta}\begin{pmatrix} +1 & 0 & -1 \\ +2 & 0 & -2 \\ +1 & 0 & -1 \end{pmatrix} * \begin{pmatrix} f_{i+1,j+1} & f_{i+1,j} & f_{i+1,j-1} \\ f_{i,j+1} & f_{i,j} & f_{i,j-1} \\ f_{i-1,j+1} & f_{i-1,j} & f_{i-1,j-1} \end{pmatrix}$$

$$\left(\frac{\partial f}{\partial y}\right)_{i,j} = \frac{1}{8\Delta}\begin{pmatrix} +1 & +2 & +1 \\ 0 & 0 & 0 \\ -1 & -2 & -1 \end{pmatrix} * \begin{pmatrix} f_{i+1,j+1} & f_{i+1,j} & f_{i+1,j-1} \\ f_{i,j+1} & f_{i,j} & f_{i,j-1} \\ f_{i-1,j+1} & f_{i-1,j} & f_{i-1,j-1} \end{pmatrix}$$

The resulting expression for the two-dimensional scalar dissipation at point (i,j) is the gradient magnitude:

$$(\nabla f \nabla f)_{i,j} = \left(\frac{\partial f}{\partial x}\right)^2_{i,j} + \left(\frac{\partial f}{\partial y}\right)^2_{i,j}$$

Using this information, we can also calculate the in-plane scalar gradient vector orientation angle ϑ

$$\vartheta = \tan^{-1}\frac{\partial f/\partial x}{\partial f/\partial y}$$

The Kolmogorov scale had been determined using the classical estimation

$$\eta = \left[\frac{\nu^3}{\varepsilon}\right]^{1/4}$$

where the dissipation rate ε was calculated both from the $k-\varepsilon$ model and from the empirical formulae $\varepsilon = 48(U_d^3/d)((x-x_0)/d)^{-4}$ obtained for free turbulent jets (see Miller and Dimotakis, 1991). Results of estimations are presented in Fig. 2 for two flow regimes both along the axis $r/D = 0$ and along the line $r/D = 0.25$. Within the distance $1 \leqslant x/D \leqslant 9$ the Kolmogorov microscale lies in the range between 30 and 300 μm what corresponds to the range of the Batchelor scales between 1 and 10 μm.

The estimates of relative uncertainty for the measurement of concentration by LIF are given in Table 2. The combined standard uncertainty was obtained from the combination between dominating uncertainties U_1 and U_2, i.e. $U_3 = \sqrt{U_1^2 + U_2^2}$. Because of the noise which is always present in any measurement system, the dissipation rate is not zero even at a constant concentration of Rhodamine. This dissipation called as the apparent dissipation rate can be estimated during the calibration measurement at a constant concentration of 0.5 mg/l using the dimensionless quantity

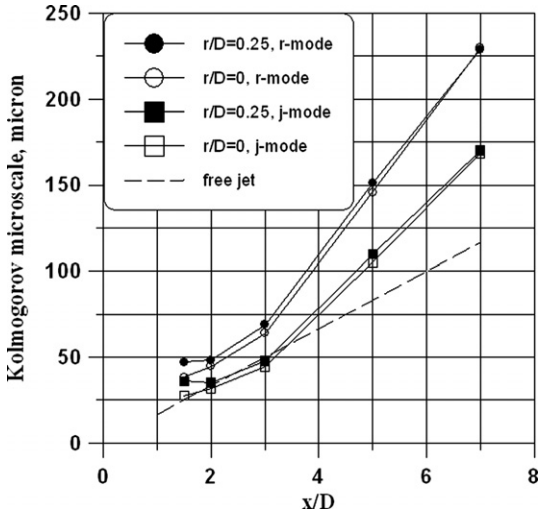

Fig. 2. Estimations of the Kolmogorov microscale $\eta = \frac{\nu^{3/4}}{\varepsilon^{1/4}}$. The dissipation rate ε is calculated from the $k-\varepsilon$ model (solid lines) and from the empirical estimation $\varepsilon = 48(U_d^3/d)((x-x_0)/d)^{-4}$ (Miller and Dimotakis, 1991).

Table 2
Relative uncertainty estimates for the calibration measurement of concentration by LIF

Designation	Parameter	Relative uncertainty (%)
U_0	Concentration	0.01
U_1	Laser power	3
U_2	Emitted and processed fluorescence signal	3.5
U_R	Combined standard uncertainty	4.6

$\hat{\chi} = \chi/(\bar{f}/D)^2]$, where $\bar{f}$ is the mixture fraction averaged in time and space over the measurement window. The mean value of $\hat{\chi}$ is about 30% of the mean value of $\hat{\chi}$ measured on the mixer axis at $x/D = 2$ and about 20% at $x/D = 9$. Unfortunately, the strong effect of noise on scalar dissipation measurements is unavoidable. Moreover, the apparent dissipation tends to dominate when the resolution increases (see, for example, Wang et al., 2007). In this paper the effects of apparent dissipation are not explicitly separated. However, the qualitative conclusions have been drawn on the base of the analysis performed for large values of the dissipation rate which are not typical for the noise (see Sections 3.6 and 3.8).

3. Results

3.1. Peculiarities of the macroflow

Topologically the flow macro structures in j- and r-modes are quite different. While the j-mode flow is very similar to the free jet, the r-mode flow exhibits two remarkable peculiarities mentioned already in Barchilon and Curtet (1964). First, the flow within the recirculation zone is highly unsteady and nearly periodic with a dominating long period mode. Long period oscillations with a dominating frequency are typical for the recirculation area where large vortex clusters are generated. They disappear in areas filled with small scale vortices and scalar structures at $x/D \geqslant 2$ and in the proximity to the mixer centerline. Second, the oscillations at symmetrical points with respect to the centerline $(r/D = 0)$ of the jet mixer are nearly antisymmetric. The flow is self-organized in such a way that the most probable event is a mixing increase at one point and a simultaneous mixing decrease at its counterpart and vice versa. This interrelation is true in the statistical sense. These facts are clearly seen in the history of the mixture fraction recorded by the PLIF method and from the analysis of the autocorrelation function of the mixture fraction fluctuations across the pipe (see Fig. 5 in Zhdanov et al., 2006).

These two flow phenomena have been thoroughly investigated and documented in our papers (see Hassel et al., 2006; Zhdanov et al., 2006; Kornev et al., 2007). However, till recent time the physical mechanism responsible for the presence of such long period antisymmetric oscillations was remaining not clear. Our latest LES calculations (see also Kornev et al., 2007) revealed that the reason for the oscillations in the recirculation zone are concentrated vortex structures arising due to instability of primary spanwise vortices. Analysis of several flow events showed that the local ejection of the scalar from the jet core towards pipe walls is preceded by the creation of concentrated vortices close to the ejection location. For instance, a three dimensional snapshot of the vortex magnitude $|\omega| = [\omega_x^2 + \omega_\theta^2 + \omega_r^2]^{1/2}$ field (Fig. 3) shows the presence of two strong vortex structures (VS) at $x/D \approx 1.7$. These can be interpreted as λ-like structures with streamwise legs put into the jet core. The structures are inclined against the main flow direction. The rotational motion inside of the structures is shown in Fig. 3 by curvilinear arrows. The structures induce the motion in the vertical direction which impacts with the pipe wall and leads to the creation of strong secondary vortices on the wall (the area S in Fig. 3). The ascending flow induced by the structures causes the

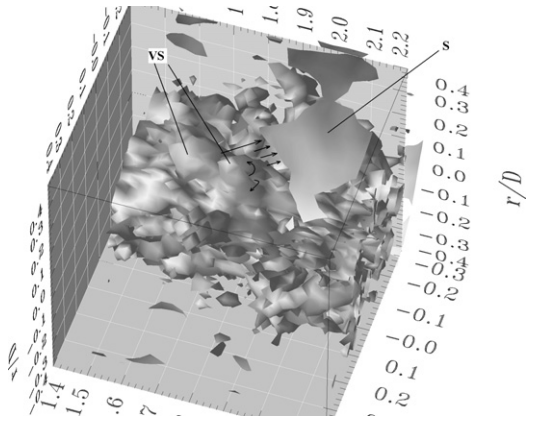

Fig. 3. Vortex structures of the flow identified as the iso-surfaces $|\omega| = \mathbf{10}^2$. VS, vortex structures; S, area of the secondary vortices at the pipe wall. LES calculation of the r-mode at $t = 27.027$ s.

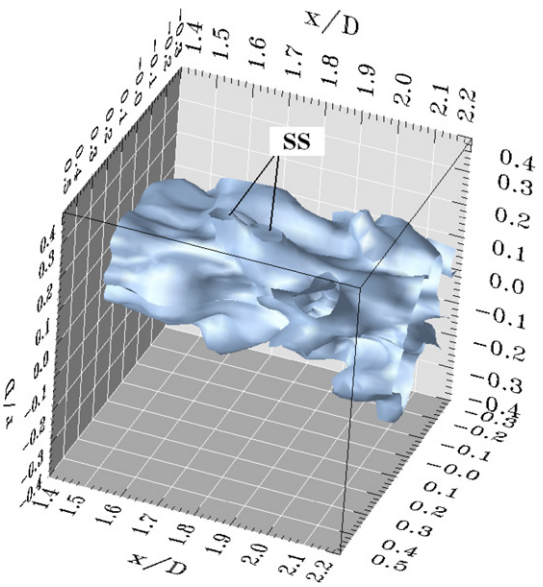

Fig. 4. Iso-surface of the mixture fraction $f = 0.425$. SS stands for scalar structure under consideration. LES calculation of the r-mode at $t = 27.027$ s.

vertical scalar flux shown in Fig. 4. The two peaks scalar structure *SS* shown in Fig. 4 indicates the strong scalar ejection, caused by the vortex VS.

The interaction between the flow and a vortex structure is schematically illustrated in Fig. 5. Through stretching effects the vortex structures can become strong and induce flow and scalar flux towards the pipe wall (Fig. 5). It leads to a scalar concentration excess near the pipe wall above the vortex structures and simultaneously to a scalar deficiency on the opposite side of the pipe. This is the reason for the phase shift of scalar fluctuations at symmetrical points with respect to the centerline.

Analysis of turbulent fluxes $\overline{u_1' f'}$ and $\overline{u_3' f'}$ supplement the description of the scalar dynamic processes gained from analysis of Figs. 3 and 4. Particularly, it was shown that the transfer of the scalar into the recirculation zone occurs mostly by back flow effects (see the flow 1 in Fig. 5) rather than by transversal transport from the central flow core (see the flow 2 in Fig. 5).

When the coflow velocity U_D increases the vortices arising in the primary jet become weaker. They are not able to induce the flow motions across and against the main flow direction which could be strong enough to overcome the coflow. The effects discussed above are weakening and the flow is changing into j-mode.

3.2. Spectrum

While Section 3.1 was devoted to large scale phenomena, in the further subsections of the paper we examine statistical properties of fine scalar structures. A sample of the spatial spectrum of scalar fluctuations shown in Fig. 6 indicates that the inertial convective range of the spectrum is well resolved for all x/D. A least-squares fit to the Kolmogorov-normalized data gives slopes -1.686 at $x/D = 2$, -1.684 at $x/D = 3$, -1.745 at $x/D = 5$, -1.73 at $x/D = 7$ and -1.68 at $x/D = 9$. These data are in agreement with well known estimation 1.71 ± 0.02 accounting for the intermittency. At large $x/D = 9$ the resolution 31 μm proved to be enough to resolve the viscous-convective subrange $E_f \sim k^{-1}$ typical for large Schmidt numbers mixing flows.

3.3. Structure of the scalar and dissipation rate fields

As mentioned above the large scale scalar structures of the j- and r-modes are quite different. The transverse scalar integral scale $L_f(r)$ defined on the mixer axis as

$$L_f(r) = \int_{-D/2}^{D/2} \frac{\overline{f'(r) f'(r+\eta)}}{\sqrt{\overline{f'^2(r)}}\sqrt{\overline{f'^2(r+\eta)}}}\, \mathrm{d}\eta,$$

where f' is the scalar oscillation and η is the separation in r direction, is growing up to $x/D \approx 3$ in both flow modes (see Fig. 7). Within the recirculation zone the structures become smaller and the integral scale is decreased at $x/D > 3$. In the j-mode the integral

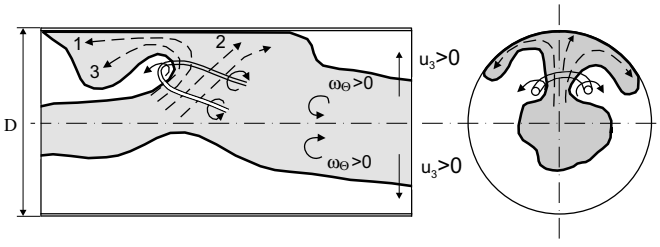

Fig. 5. Schematic representation of scalar flux induced by vortex structures.

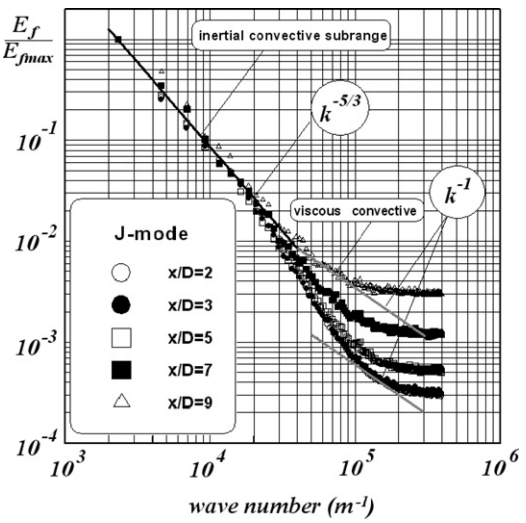

Fig. 6. Scalar spectrum at different x/D along the mixer centerline (j-mode).

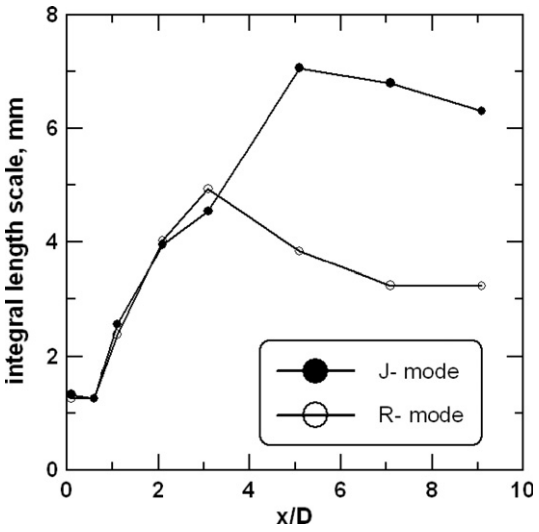

Fig. 7. Distribution of the scalar integral length along the axis.

scale is continuing to grow up to $x/D \approx 7$, where the strong interaction between the jet and the pipe wall takes place, and then decreases. This evolution is reflected in sample fields shown in Figs. 8 and 9. The size of structures shown in Fig. 8–10 are sufficiently smaller than the integral lengths (Fig. 7) and therefore they can be classified as the microstructures of the turbulent scalar field. While scalar layers with thickness of a few dozen microns can be recognized in the j-mode at $x/D = 7.0$ (Fig. 9b), the scalar field in the r-mode (Fig. 8d) seems to be fully smoothed already at $x/D = 5.0$. However, as shown below, the fine scalar structures have certain similar statistical properties in both flow modes. The dissipation rate $\chi = D_i \nabla f \nabla f(x, y, t)$, where D_i is the scalar diffusivity, maps provide more contrast and allowing the structures to be more readily seen. The scalar dissipation rate is concentrated in thin dissipation layers (see Fig. 10). Three fundamental topologies, introduced in Buch and Dahm (1996), can be identified in the scalar field. They include long regions consisting of many straight and nearly parallel dissipation layers, areas where two such long regions meet orthogonally and spiral structures (see Fig. 10).

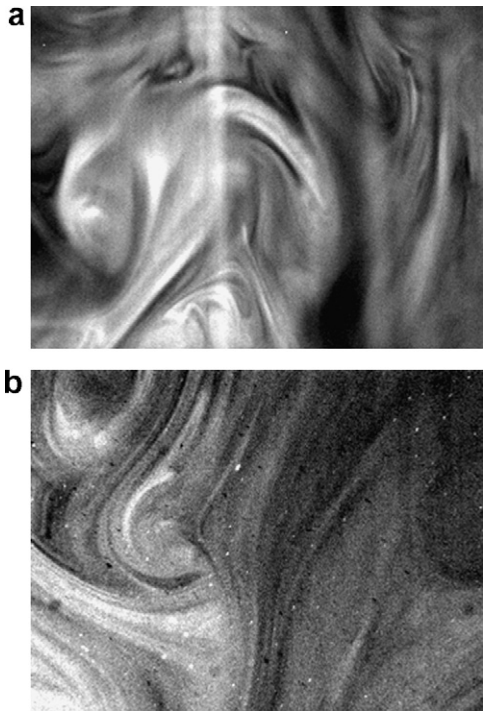

Fig. 9. Sample planes in the j-mode: (a) $x/D = 3.0$ and (b) $x/D = 7.0$. The actual size of the windows is 2.74×2.075 mm whereas the corresponding integral lengths are: (a) 4.5 mm and (b) 6.8 mm.

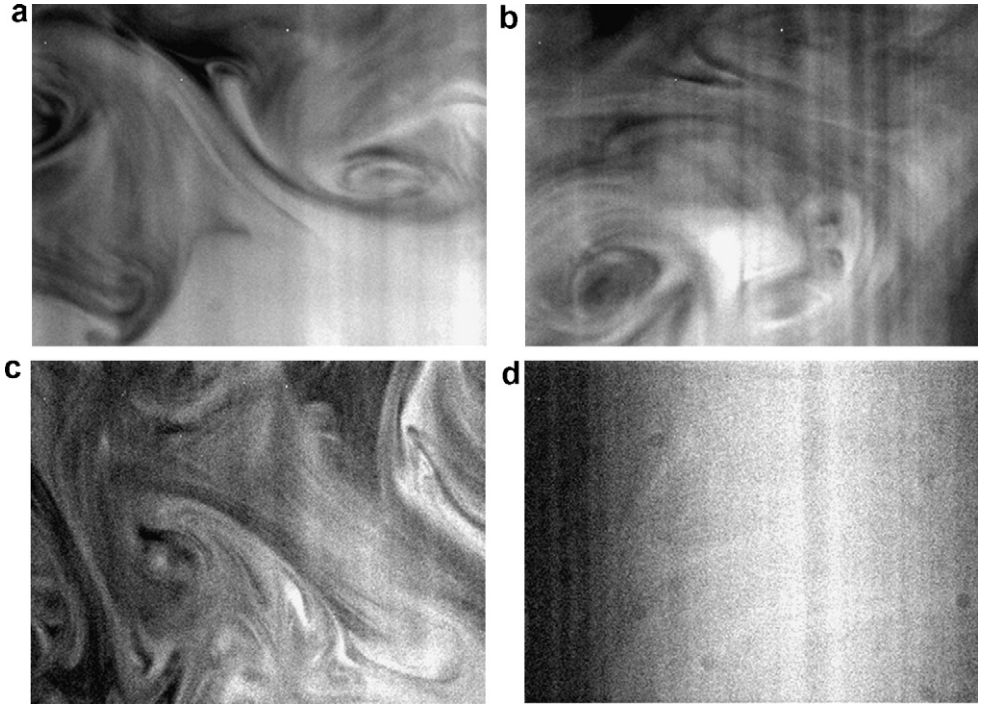

Fig. 8. Sample planes at $r/D = 0$ in the r-mode: (a) $x/D = 1.0$; (b) $x/D = 1.5$; (c) $x/D = 3.0$ and (d) $x/D = 5.0$. The actual size of the windows is 2.74×2.075 mm whereas the corresponding integral lengths are: (a) 2.4 mm; (b) 3.2 mm; (c) 4.9 mm and (d) 3.8 mm.

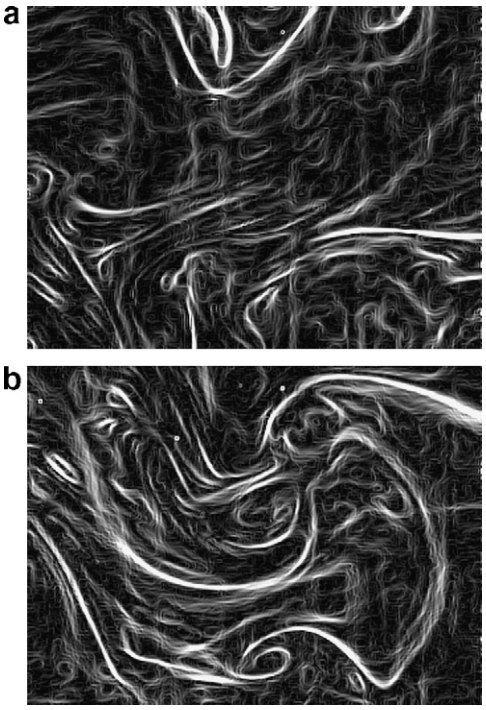

Fig. 10. 2D Scalar dissipation rate $\chi = (\frac{\partial f}{\partial x})^2 + (\frac{\partial f}{\partial y})^2$ on the centerline at $x/D = 2$ in the r-mode. The actual size of the windows is 2.74×2.075 mm whereas the corresponding integral length is 4 mm.

3.4. Cumulative distributions and probability densities of the dissipation rate

Fig. 11 shows the fraction of the total data volume in which the local scalar dissipation rate is greater than some threshold value χ (see Buch and Dahm, 1996), namely $A_0(\chi) = \int dA_{\chi'>\chi}/dA$, where A is the measurement window area. The rapid drop of A_0, called as the cumulative distribution function (c.d.f), at very low values of χ reflects the fact that the scalar dissipation field is composed primarily of very low values, with high vales occurring infrequently (see Buch and Dahm, 1996). Notice that c.d.f. depends weakly both on the flow mode and on x/D. The same conclusion can be drawn from the consideration of the p.d.f. of the $\log_{10}[\chi/(\bar{f}/D)^2]$ (see Fig. 12),

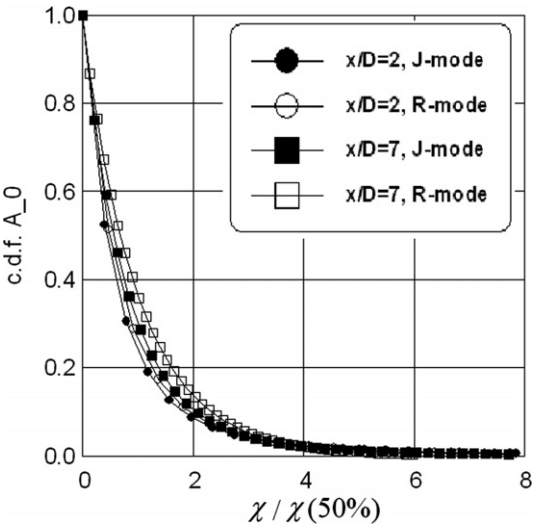

Fig. 11. The cumulative distribution function of scalar dissipation rates versus χ normalized with the corresponding measured median dissipation value $\chi_{50\%}$.

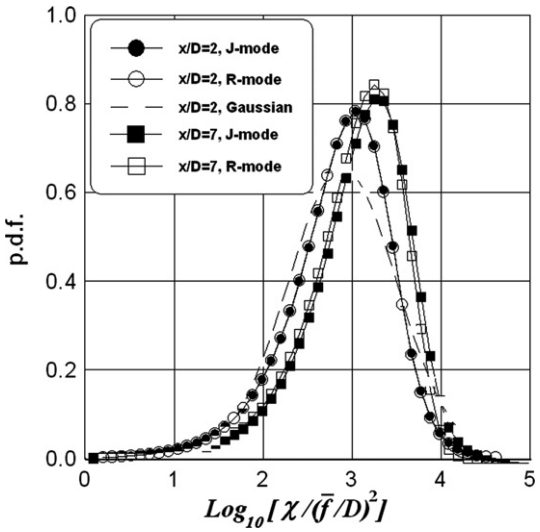

Fig. 12. The PDF of the logarithm of the scalar dissipation rate χ.

where $\bar{f}$ is the mixture fraction averaged in time and space over the measurement window. The curves artificially centred on the same mean value of $\log_{10}[\chi/(\bar{f}/D)^2]$ are almost the same for both flow modes. Typical deviations between the experimental data and the Gaussian distribution having the same two first moments (the log-normality law of Gurvich and Yaglom, 1967) are observed. The scalar dissipation rate clearly departs from the log-normality. An interesting result of this study is that the similarity laws of the scalar microstructures (e.g. the similarity laws for c.d.f. and p.d.f.) revealed in highly resolved measurements performed by Buch and Dahm (1996) for shear flows hold true in our study although we did not resolve the smallest (Batchelor) scales of the scalar field. Obviously, universality of fine scalar structures takes place at scales sufficiently larger than the Batchelor ones.

3.5. Intermittency

A remarkable feature of the scalar field is the presence of areas with a rapid change of the scalar. These structures called cliffs can easily be seen in Fig. 13. They cause the small-scale intermittency (Warhaft, 2000). As a result, the scalar difference $\Delta f(r) = f(r) - f(0)$

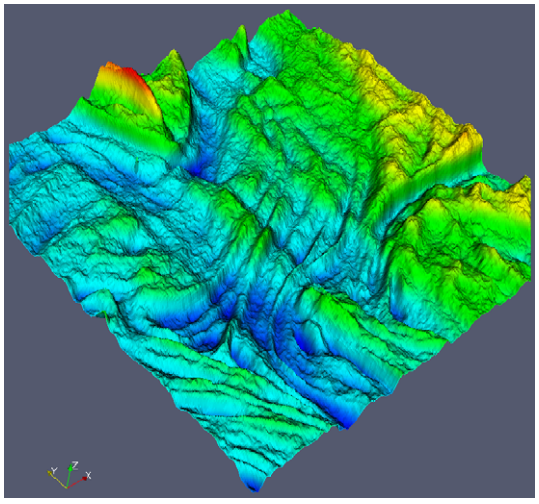

Fig. 13. A snapshot of the scalar distribution within the measurement window. $x/D = 2$, r-mode.

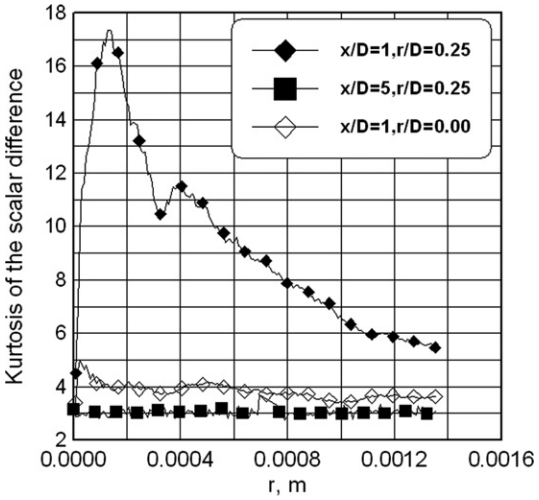

Fig. 14. The kurtosis of the scalar difference $\Delta f(r) = f(r) - f(0)$ for the r-mode as a function of the separation r.

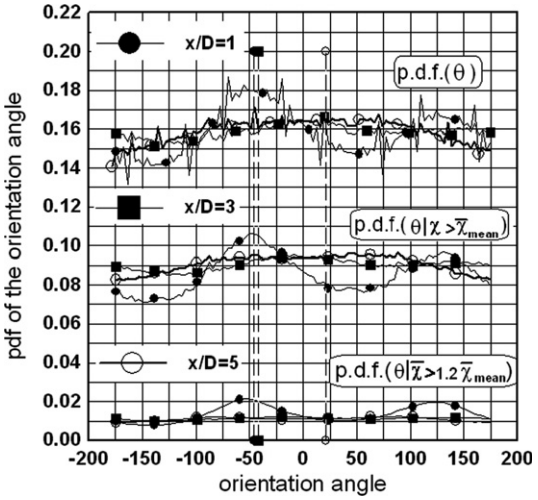

Fig. 16. The distribution of the scalar gradient orientation angles at $r/D = 0.25$, r-mode. The vertical dot lines show the orientation of the most compressive mean strain axis.

(the structure function of the first order) statistics is non Gaussian and the intermittency is observed at inertial range scales (Fig. 14). The intermittency is most pronounced in the front part of the recirculation zone at $x/D = 1$ and $r/D = 0.25$. In the well mixed stage at $x/D > 3$ in the r-mode the scalar difference statistics is almost Gaussian. In the j-mode the intermittency on the centerline is observed up to $x/D = 9$. On the centerline $r/d = 0$ the intermittency is less than at $r/d = 0.25$ for both flow modes. In all measurements the kurtosis tends to the Gaussian value of three at large scales and at scales corresponding approximately to the end of the inertial range. Most likely, the latter can be explained by insufficient resolution and noise in the PLIF data.

3.6. Small-scale anisotropy and orientation of the scalar structures

Anisotropy at high *Sc* numbers is an important topic for the development of LES SGS (subgrid stress) models. Small-scale anisotropy is assessed by testing if the measured scalar gradient vector $\nabla f(x, r, t)$ shows any preferred orientation within the measurement plane. For that, the p.d.f. distribution of the angle $\vartheta = \tan^{-1} \frac{\partial f/\partial y}{\partial f/\partial x}$ measured in the (x, r)-plane from the x-axis has been examined. The results are shown in Figs. 15 and 16 at different x/D

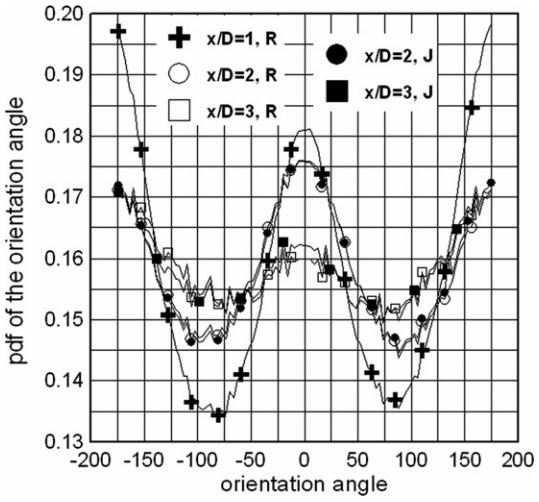

Fig. 15. The distribution of the scalar gradient orientation angles at different x/D and $r/D = 0$.

along the mixer centerline both in the r- and the j-modes. If the underlying fields $\nabla f(x, r, t)$ were fully isotropic then the distribution of ϑ-values should appear uniform (see Buch and Dahm, 1996). Notice that despite of a quite different structure of the macro flow in the r- and the j-mode the p.d.f. distributions of ϑ is independent of the flow mode. The mean flow at $r/D = 0$ has its principal compressive strain axis lying along the mixer centerline. Therefore, it is quite understandable from physical point of view, that the p.d.f. distribution has two peaks at $\vartheta = 0$ and $\vartheta = \pm\pi$. At $x/D = 1$ and $x/D > 2$ the most preferred orientation is $\vartheta = \pm\pi$ what is quite expectable since the orientation angle of the mean scalar gradient $\partial\bar{f}/\partial x \leqslant 0$ is $\pm\pi$. However, at $x/D = 2$ the orientations $\vartheta = 0$ and $\vartheta = \pm\pi$ are equally preferred. This is the flow zone where the compressive effects $\partial\bar{u}/\partial x \leqslant 0$ causing the equivalence of the directions $\vartheta = 0$ and $\vartheta = \pm\pi$ are very large whereas the mean scalar gradient $\partial\bar{f}/\partial x \leqslant 0$ responsible for the preference of the direction $\vartheta = \pm\pi$ is sufficiently weakened in comparison with that in the section $x/D = 1$ (see Fig. 5a and b in Zhdanov et al., 2006). At $x/D > 2$ the scalar gradient field is very nearly isotropic with a slight preference of the gradient vector to align with the most compressive strain axis and the mean scalar gradient. Fig. 16 shows the gradient vector orientation angles at $r/D = 0.25$ in the r-mode. The most pronounced anisotropy is detected in the front part of the recirculation zone at $x/D = 1$ whereas at $x/D > 2$ the scalar field is nearly isotropic. The distributions were calculated for all possible scalar gradients vectors (p.d.f. (ϑ)), for all vectors corresponding to the dissipation rates larger than the mean dissipation rate χ_m (p.d.f. $(\vartheta|\chi > \chi_m)$) and for the vectors corresponding to the dissipation rates larger than $1.2\chi_m$ (p.d.f. $(\vartheta|\chi > 1.2\chi_m)$). Such analysis is necessary from two reasons. First, the layers which are orthogonal to the measurement plane are separated from the layers which are oriented at an oblique angle to the laser sheet. Indeed, the thin high-dissipation layers are oriented approximately normal to the measurement plane because a layer that was oriented at an oblique angle with respect to the laser sheet would appear thicker and exhibit lower dissipation. In so doing the disadvantages of the PLIF measurement providing only 2D information can be mitigated. Second, the small structures with high dissipations are separated from large ones which are always present in the recirculation zone. The results show clearly that at $x/D = 1$ the gradient vector of scalar structures corresponding to different dissipation rates has the preferential direction at approximately $\vartheta \approx -50^\circ$ what is in agreement with the orientation of the

most compressive strain axis $\vartheta_{sa} \approx -46^\circ$ gained from our LES. The orientation of the mean scalar gradient $\vartheta_m = \tan^{-1}\frac{\partial \bar{f}/\partial y}{\partial \bar{f}/\partial x} \approx -75^\circ$ differs from ϑ. Like in the case $r/D = 0$, the scalar gradient field at $r/D = 0.25$ becomes isotropic at large x/D. However, there exists a preferential orientation of the scalar gradient vector which agrees well with the orientation of the most compressive strain axis ($\vartheta_{sa} \approx -42^\circ$ at $x/D = 3$ and $\vartheta_{sa} \approx 21^\circ$ at $x/D = 5$). No correlation is found between ϑ and ϑ_m.

3.7. Contribution of different scales to the scalar variance

Consideration of *Sc* number effects in mixing models is the problem which is still far from its solution. The variance of the mixture fraction in liquid mixtures should be larger than in gas mixtures since the diffusion effects characterized by the Schmidt number are sufficiently less in liquids than in gases. This fact which is beyond doubts is explicitly used in the multiple-time-scale (MTS) turbulent mixing model proposed by Baldyga and Bourne (1999). The local variance $\sigma = \overline{(f - \bar{f})^2}$ is represented as the sum of three terms σ_1, σ_2 and σ_3 corresponding to the inertial-convective (σ_1), viscous-convective (σ_2) and viscous-diffusive (σ_3) ranges of the scalar spectrum $E_f(k)$. Results calculated using the MTS model (see Chorny et al., 2008) are presented in Fig. 17. The PLIF data obtained in our previous work (Zhdanov et al., 2006) with the resolution of 300 μm being at $x/D = 9$, 30 times larger than the Batchelor scale agree relatively well with the LES results. LES was performed with use of the dynamic mixed SGS models (see Tkatchenko et al., 2007) developed regardless of the *Sc* number effects. At first glance the large discrepancy between LES, PLIF and MTS model can be explained by the insufficient resolution of PLIF measurements and by gaps in SGS modelling. One could expect that the tenfold increasing the resolution in the present PLIF measurements should result in a sufficient increase of the mixture fraction variance and in the reduction of the discrepancy between MTS and PLIF data. However, new PLIF data are proved to be very close to the old ones and they agree satisfactory with the LES. Substantial decrease of the variance at large x/D can be explained by tenfold increased Rhodamine concentration used in fine PLIF measurements. In this case the noise to signal ratio is substantially less and new PLIF data are more accurate. Most likely the reason for the satisfactory agreement between LES and measurements is, that the dominating contribution to the scalar variance is made by large scale oscillations corresponding to the energy containing and inertial convective subranges of the spectrum. The contribution from oscillations with scales of a few Batchelor lengths, which were not resolved in the first PLIF series and not taken into account in the SGS LES models, is minor, i.e $\sigma_1 \gg \sigma_2$ and $\sigma_1 \gg \sigma_3$. Obviously, this is the reason why the LES models originally developed for the case $Sc \sim 1$ provide quite reasonable results for the scalar variance in liquid mixtures. The discrepancy between the RANS MTS model and measurements can be explained by general disadvantages of the RANS technique compared with LES (see Tkatchenko et al., 2007) and by sufficient overestimation of σ_2 and σ_3 contributions in the MTS model.

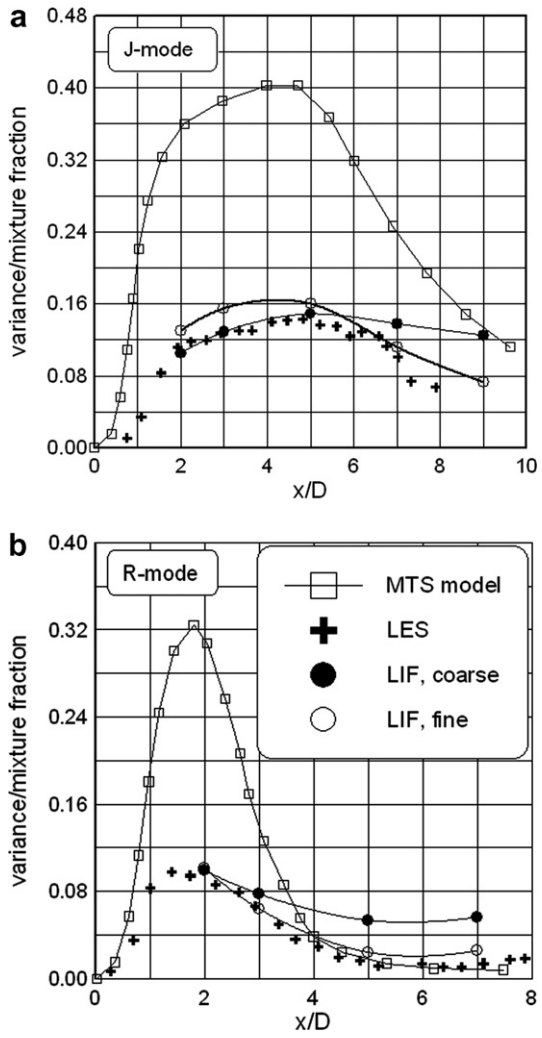

Fig. 17. Mixture fraction variance versus x/D for j- and r-modes. LIF, coarse – measurement with resolution of 300 μm (Zhdanov et al., 2006); LIF, fine – present measurements.

3.8. Fractal properties: multiplier distributions

This part of the work has been motivated by a recent development of LES SGS models utilizing the multifractal properties of the turbulence (see Burton et al., 2002). We examine the multiplier distributions introduced by Novikov (1971). Let us consider a positive stochastic function of the turbulent flow $y(x)$ and the fractional coefficient $q_{r,l}$ defined by the condition

$$q_{r,l}(h,x) = y_r(x_1)/y_l(x), \tag{1}$$

where

$$y_l(x) = \frac{1}{l}\int_{x-l/2}^{x+l/2} y(x_1)\,dx_1, \qquad -0.5 \leqslant h = \frac{x_1 - x}{l - r} \leqslant 0.5, \quad r < l. \tag{2}$$

It is assumed that the function $y(x)$ is locally homogeneous and isotropic at scales smaller than a certain integral length scale L_u and there exists the second characteristic scale l_* determined either by the viscosity or by the diffusion. If in the range between l_* and L_u there are no other characteristic scales influencing the stochastic function $y(x)$, then the probability density function of the fractional coefficient $q_{r,l}$ depends only on the ratio l/r and $|h|$ provided l and r satisfy the condition $L \gg l > r \gg l_*$. A very strong assumption of the Novikov's theory is the statistical independency of the consecutive fractional coefficients

$$\overline{q_{r,\rho}(h, x + h(l-\rho))q_{\rho,l}(h,x)} = 0, \tag{3}$$

where $r < \rho < l$ at scales between l_* and L_u. The scale similarity postulated by Novikov implies the multifractal nature of the turbulence closely related to the cascade concept (Jimenez, 2000).

The Novikov's concept has then been used in a series of works on multifractals in turbulence (see Chhabra and Sreenivasan, 1992). The usual procedure which is also applied in the present paper is the consideration of a hierarchy of parents and children

boxes of uniform size. Each parent box with the size p is subdivided into a number of children boxes, κ with sizes $p_1 = p/\kappa$, and the ratios of the dissipation rates in the original box to those in the children sub-boxes are computed. A histogram of these ratios is then $P(M)$. According to the Novikov's concept the shape of the distribution $P(M)$ should remain invariant for the inertial range of scales. This fact is used for the development of the LES SGS models (Burton et al., 2002). Unfortunately, the invariance has not been supported in our measurements.

We used two ways to cover the measurement window by a hierarchy of boxes (see Fig. 18). In the first one, the window is successively subdivided into square boxes of equal size each of which is then bisected into two children boxes (a simple binomial cascade) (see Fig. 18a–c). The ratio

$$M = \int_{\text{child}} \chi(s)\,\mathrm{d}s \Big/ \int_{\text{parent}} \chi(s)\,\mathrm{d}s, \tag{4}$$

computed for every couple of equal size p, contributes to the total probability density function $P(M)$. In the second way, the hierarchy contains enclosed boxes (see Fig. 18d).

Due to the influence of the noise the probability density function $P(M)$ is of the Gaussian type with very small values at ends of the range $M \in [0, 1]$. To reduce the effect of the noise the probability density function $P(M)$ was computed only for dissipation rate values larger than a certain threshold $\chi_t = 10^4$. The threshold $\chi_t = 10^4$ corresponds to the maximum dissipation rate gained from the calibration measurements with Rhodamine solutions of the constant concentration. At ideal conditions without the noise χ_t should be zero. The multiplier distributions $P(M)$ computed for boxes of different sizes $250 < p < 1000$ μm corresponding to the inertial range (see Fig. 6) are proved to be dependent on the box size p (see Fig. 19). There takes place a flattening of curves when p becomes less, i.e. a irregular distribution of χ becomes more and more probable when the size of the parent box gets less. Unfortunately, the multiplier distributions $P(M)$ computed for different p are not universal and varied along the mixer axis (Fig. 20). At large distances where the mixing is close to be completed the probability distribution tends to the Gaussian one. The intermittent character of the scalar distribution is sufficiently weakened. The results presented in Figs. 19 and 20 confirm the intermittent character of the scalar distribution especially in flow areas of strong mixing at small x/D. Unfortunately, the Novikov's cascade model idea (Novikov, 1971) has not been supported in our measurements. This conclusion is regardless of the choice of box sets used for calculation of the multiplier distributions.

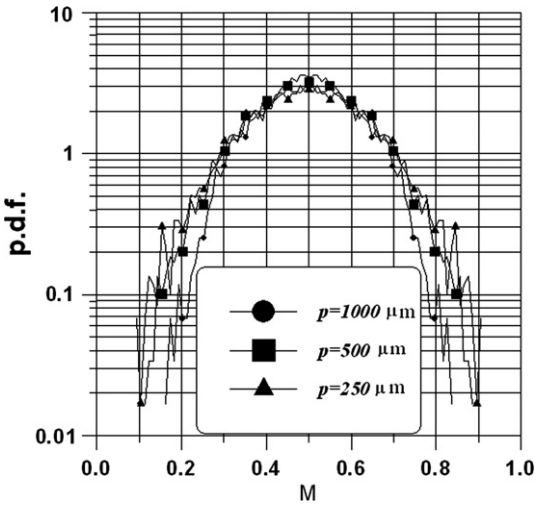

Fig. 19. Multiplier distributions $P(M)$ for different box sizes p. $x/D = 2$, j-mode.

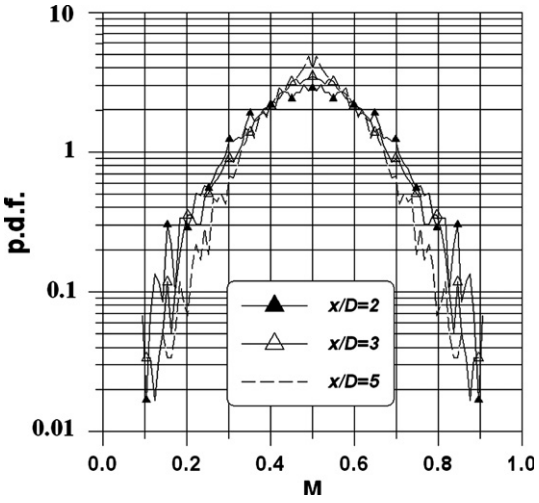

Fig. 20. Multiplier distributions $P(M)$ for different cross-sections x/D along the mixer axis in the j-mode. Box size $p = 250$ μm.

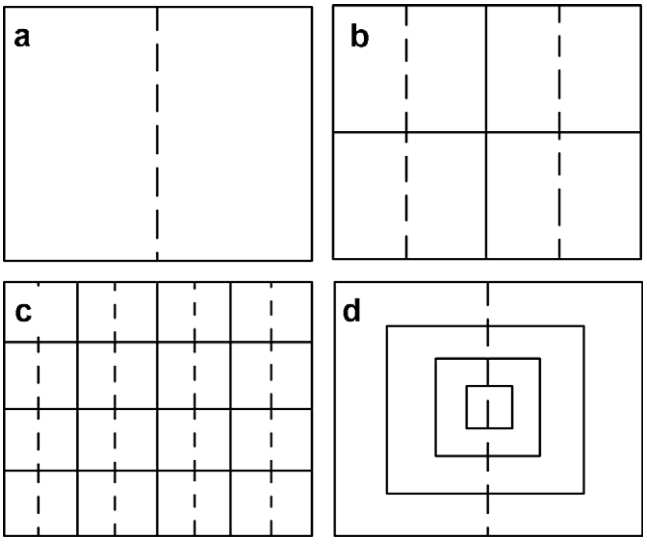

Fig. 18. Parent–children box sets used for calculation of the multiplier distributions.

Since the inertial range has been reliably resolved (see Fig. 6) the only possible explanation for the contradiction between our experimental data and the Novikov's theory can be the failure of the assumption (3). Indeed, the statistical analysis of correlations between the successive fractional coefficients (4) reveals a strong statistical dependency among them. A possible explanation for this fact can be found in Jimenez (2000). As mentioned in Jimenez (2000) there exist elongated coherent objects (vortices) in every turbulent flow which are difficult to classify into cascade steps. They span the full range of the cascade and part of the cascade is blocked. This physical mechanism is referred to as the blocking effect (Jimenez, 2000). The same physical mechanism can be used for explanation of our experimental observations. Obviously, there exist scalar coherent structures which are themselves not cascading. They are present in all boxes of the inertial range regardless of the size p. As a result, the fractional coefficients (4) belonging to different levels of the binomial cascade are statistically dependent on

one another. That is why the multiplier distributions $P(M)$ are not invariant.

4. Conclusions

The macrostructures of the flow in a confined jet configuration depend strongly on the flow mode. In the j-mode the structures are similar to those of the free jet. In the r-mode the coherent vortex structures with dominant streamwise components of vorticity cause oscillations containing a dominating long period mode. These structures arising periodically in the primary nozzle jet cause scalar ejections towards the pipe wall and propagation of the scalar against the main flow. Due to the vortex induced transversal and axial motions the scalar concentration increases on one side of the pipe and decreases on the opposite one. As a result the phase shift of scalar fluctuations is observed at symmetrical points with respect to the pipe centerline. Schematically, a typical scenario which leads to the phase shifted scalar oscillations is shown in Fig. 5. These vortex structures become weaker as the coflow velocity U_D increases and the flow is changing into j-mode.

The fine scalar structures with scales sufficiently less than the integral scale are strongly influenced by large scale motions. For instance, in the r-mode the fine structures become smaller behind the recirculation zone and are difficult to recognize visually at the end of the test section. On the contrary, in the j-mode the fine structures can be clearly identified up to $x/D = 7$. Topologically the fine structures in both flow modes are similar. The scalar dissipation rate is concentrated in thin dissipation layers having the form of long regions consisting of many straight and nearly parallel dissipation layers, spiral structures and saddle- type structures. Despite of the big difference in the structure of the macroflow and in the dynamics of fine structures there exist statistical properties which are very similar for both flow modes. For instance, the normalized cumulative distributions and probability densities of the dissipation rate are almost the same for all flow modes. There is a clear departure of the scalar dissipation rate χ from the log-normality law.

A remarkable feature of the scalar field is the presence of structures with a rapid change of the scalar. These structures called cliffs cause small-scale intermittency which is strongly dependent on the flow mode. The intermittency is most pronounced in the front of the recirculation zone and becomes weaker on the centerline and downstream. In a well mixed stage the scalar field has Gaussian statistics. Every individual scalar structure exhibits a pronounced anisotropy. However, the collective statistics of fine scalar structures can be considered as nearly isotropic. For instance, the orientation of the scalar gradient is more or less uniform in space with a slight preference to align with the direction of the most compressive mean strain axis. For the flow under consideration the most contribution to the scalar variance is made by large scale motions whereas the contribution of fine scales smaller than typical inertial range scales is negligible. This is the reason why the LES models originally developed for the case $Sc \sim 1$ provide quite reasonable results for the scalar variance in liquid mixtures at $Sc \sim 10^3$. Study of the multiplier distributions confirms the fact that the dissipation rate is distributed very unevenly in space. However, the Novikov's cascade model idea (Novikov, 1971) has not been supported in our measurements.

Acknowledgement

The authors acknowledge gratefully the support of the German Research Foundation (DFG) through the program SPP 1141. LES calculations have been performed on IBM pSeries 690 Supercomputer at the North German Alliance for the Advancement of High-Performance Computing (HLRN).

References

Baldyga, J., Bourne, J.R., 1999. Turbulent Mixing and Chemical Reactions. John Wiley and Sons.
Barchilon, M., Curtet, R., 1964. Some details of the structure of an axisymmetric confined jet with backflow. J. Basic Eng., 777–787.
Buch, K.A., Dahm, W.J.A., 1996. Experimental study of the fine-scale structure of conserved scalar mixing in turbulent shear flows. J. Fluid Mech. 317, 21–71.
Burton, G.C., Dahm, W.J.A., Dowling, D.R., Powell, K.G., 2002. A new multifractal subgrid-scale model for large-eddy simulation. AIAA Paper 2002-0983.
Chhabra, A.B., Sreenivasan, K.R., 1992. Scale-invariant multiplier distributions in turbulence. Phys. Rev. Lett. 68 (18), 2762–2765.
Chorny, A.D., Kornev, N.V., Hassel, E., 2008. Simulation of the passive scalar mixing in the jet mixer. J. Engineering Physics and Thermophys. 81 (4), 693–705.
Gurvich, A.S., Yaglom, A.M., 1967. Breakdown of eddies and probability distributions for small-scale turbulence, boundary layers and turbulence. Phys. Fluids Suppl. 10, 59–65.
Hassel, E., Jahnke, S., Kornev, N., Tkatchenko, I., Zhdanov, V., 2006. Large-Eddy Simulation and laser diagnostic measurements of mixing in a coaxial jet mixer. Chem. Eng. Sci. 61, 2908–2912.
Jimenez, J., 2000. Intermittency and cascades. J. Fluid Mech. 409, 99–120.
Kornev, N., Tkatchenko, I., Zhdanov, V., Hassel, E., Jahnke, S., 2005. Simulation and measurement of flow phenomena in a coaxial jet mixer. In: Humphrey, J.A.C. (Ed.), Proceedings, 4th International Symposium Turbulence and Shear Flow Phenomena, Williamsburg, VA, vol. 2, 2005, pp. 23–728.
Kornev, N., Tkatchenko, I., Zhdanov, V., Hassel, E., Jahnke, S., 2007. LES simulation and measurement of separation flow phenomena in a confined coaxial jet with large inner to outer velocity ratio. Adv. Appl. Fluid Dyn. 2 (1), 1–28.
Kushnir, D., Schumacher, J., Brandt, A., 2006. Geometry of intensive scalar dissipation events in turbulence. Phys. Rev. Lett. 97, 124502.
Lima, M., Palma, J., 2002. Mixing in coaxial confined jets of large velocity ratio. In: Proceedings, 10th International Symposium on Application of Laser Technique in Fluid Mechanics, Lisboa, 8–11 July 2002.
Miller, P.L., Dimotakis, P.E., 1991. Reynolds number dependence of scalar fluctuations in a high Schmidt number turbulent jet. Phys. Fluids A 3, 1156–1163.
Mortensen, M., Orciuch, W., Bouaifi, M., Andersson, B., 2003. Mixing of a jet in a pipe. Trans. IChemE 81A, 1–7.
Novikov, E.A., 1971. Intermittency and scale similarity of the turbulent flow structure. Appl. Math. Mech. 35 (2), 266–277.
Rehab, B., Villermaux, E., Hopfinger, E., 1997. Flow regimes of large-velocity-ratio coaxial jet. J. Fluid Mech. 345, 357–381.
Schumacher, J., Sreenivasan, K.R., 2005. Statistics and geometry of passive scalars in turbulence. Phys. Fluids 17 (12), 125107.
Southerland, K.B., Dahm, W.J.A., 1994. A four-dimensional experimental study of conserved scalar mixing in turbulent flows. Tech. Rep. 026779-12, University of Michigan.
Su, L.K., Clemens, N.T., 2003. The structure of fine-scale scalar mixing in gas-phase planar turbulent jets. J. Fluid Mech. 488, 1–29.
Tkatchenko, I., Kornev, N., Jahnke, S., Steffen, G., Hassel, E., 2007. Performances of LES and RANS models for simulation of complex flows in a coaxial jet mixer. Flow Turbul. Combust. 78, 111–127.
Wang, G.H., Clemens, N.T., Barlow, R.S., Varghese, P.L., 2007. A system model for assessing scalar dissipation measurement accuracy in turbulent flows. Meas. Sci. Technol. 18, 1287–1303.
Warhaft, Z., 2000. Passive scalars in turbulent flows. Ann. Rev. Fluid Mech. 32, 203–240.
Zhdanov, V., Kornev, N., Hassel, E., Chorny, A., 2006. Mixing of confined coaxial flows. Int. J. Heat Mass Transf. 49, 3942–3956.